International Journal on
"Technical and Physical Problems of Engineering"
(IJTPE)
Published by International Organization of IOTPE

ISSN 2077-3528
IJTPE Journal
www.iotpe.com
ijtpe@iotpe.com

September 2024	Issue 60	Volume 16	Number 3	Pages 203-212

MIXED CONVECTION INVESTIGATION OF A HEATING BLOCK WITHIN A LID-DRIVEN CUBIC CAVITY FILLED WITH NANOFLUID

A. Siadi [1] L. Belarche [1] B. Abourida [2] K. Bouzid [1]

1. Laboratory of Mechanics, Processes, Energy and Environment (LMPEE), National School of Applied Sciences, Ibn Zohr University, Agadir, Morocco, ali.siadi@edu.uiz.ac.ma, l.belarche@uiz.ac.ma, kamal.bouzid@edu.uiz.ac.ma
2. Laboratory of Fluid Mechanics and Energy, Faculty of Sciences, Cadi Ayyad University, Marrakech, Morocco b.abourida@uiz.ac.ma

Abstract- The ultimate objective of this investigation is to analyze the effect of the block's dimension ratio and lid movement on the fluid movement and transfer of heat in an alumina nanofluid filled lid driven cubic cavity (alum-water). The enclosure's right side has an isothermal block, The lid on the left side moves with a speed V_0 and is maintained at a low temperature. T_c while every wall that remains is adiabatic. The Finite volume approach and the Bossiness approximation are accustomed to discretize then work out the regulating equations. The end results of the numerical calculations are displayed as streamlines, isotherms, and Nusselt numbers for many thermal parameters, namely, Reynolds numbers ($10 \leq R_e \leq 200$), Richardson numbers ($0.1 \leq R_i \leq 10$), particle volume fraction ($0\% \leq \Phi \leq 4\%$) and different block dimensions ($20\% \leq \varepsilon \leq 70\%$) with respect to the cavity size. The results indicated that there is an enhancement in heat transmission as a result of a growth in Reynolds numbers and the volume fraction of nano-fluid particles. Additionally, results were obtained when altering the block's dimensions within the examined configuration.

Keywords: Lid-Driven, Mixed Convection, Nano-Fluid, Three-Dimensional, Finite Volume Method.

1. INTRODUCTION

Mixed convection, resulting from the combination of natural convection and forced convection, constitutes a captivating field in thermos fluid dynamics with significant implications in various sectors. It plays a crucial role in heat dissipation and offers opportunities for optimization in energy performance and thermal system design. Mixed convection aims to highlight its versatility and influence by paving the way for innovative advances in its application areas such as industrial cooling systems, energy-related technologies, the design of electronic components, heating and cooling processes, as well as in more specific applications like solar panels and heat recovery devices. Many investigations have been conducted regarding heat transfer through mixed convection in simple and complex cavities under various thermal and kinematic boundary conditions.

Ben Cheikh, et al. [1] employed a finite volume schema coupled with a multi grid technique to conduct a numerical search of natural convection in a non-uniformly heated square-cavity. The hollow was filled with various nano-fluids containing nanoparticles of Ag, Cu, Al_2O_3, and T_iO_2. The researchers focused on analyzing the heat transference characteristics and observed how they were influenced by the volume fraction of nanoparticles on them and the category of fluid nano-particles. The outcomes of their study revealed that higher nano-particle volume fractions resulted a growth in the rate of heat exchange for all Rayleigh numbers considered. However, they additionally discovered that temperature exchange enhancement was strongly depending upon the specific type of nano-fluid used. Specifically, a maximal transfer of heat rate was noted by the researchers when using Cu or Ag nanoparticles, while the minimum heat transference rate was observed when TiO_2 nanoparticles were employed.

In their study, Doshmanziari, et al. [2] focused on examining The properties of heat transmission of Al_2O_3-water nano-fluid. Their findings indicated that the rate of heat transfer improved as a result of the introduction of nanoparticles. by up to 14%. This observation aligns with numerous experimental studies that have demonstrated the potential for enhancing thermal conductivity through the utilization of nano-fluids. Messaoud and his colleagues [3] executed a mixed-convection numerical study in various transversely shaped concave enclosure. They observed the triangular enclosure exhibits a higher heat transfer rate at higher Reynolds number.

Fontana, et al. [4] investigated the primary properties of MXD-convection in incompletely open chambers with Inside-in sources of heat. The results demonstrate that buoyancy forces predominate for low Reynolds and Rayleigh values, and in this instance, the flow field corresponds to two recirculation's revolving as opposed to one another. Iwatsu, et al. [5] examined conducted a numerical analysis of MXD-Convection heat exchange in a driven enclosure subjected to a stable vertical temperature gradient.

Registered: 240228 Article Info: 1851 Accepted: 240814
Reserved: 240528 Available: 240930

Their results indicate that the current characteristics are like to those observed in a conformist enclosure subjected to a non-stratified fluid when Richardson number values are low. Additionally, it was detected that at very high Richardson number values, a significant portion of the central and lower regions inside the cavity remains stagnant.

Doghmi, et al. [6] recently carried out a 3-D numerical analyzesis to explore the influence of the size of the inlet opening on MXD-Convection within a ventilated hollow. Their findings suggest that as Richardson numbers increase, the Nusselt number average at the active walls exhibits a concurrent increase. Moreover, they observed that increasing the inlet opening section leads to an increase in heat transfer rate at the hot wall and a decrease at the cold wall.

Abu Nada, et al. [7] conducted an investigation on the mixed-convection phenomenon occurring within inclined square cavities driven by a moving lid. The cavities were full of with a nano-fluid composed of water and Al_2O_3 nanoparticles. The findings of the study revealed that the flow characteristics and heat exchange mechanisms were suggestively influenced by the Richardson number, which is a dimensionless parameter related to the balance between buoyancy and inertial forces. The results shed light on the complex interchange between buoyancy driven and L. DRVN flows, providing insights into the heat transfer enhancement mechanisms within the nano-fluid filled cavities.

In their research, Sheremet and Pop [8]. Was conducted a numerical simulation to investigate study laminar MXD-Convection in a hollow driven by a single or double lid. The cavity was full of nano-fluid consisting of nanoparticles Al_2O_3 and water. The aim of the study was to analyze the flow and warmness exchange characteristics under these conditions. Nouari, et al. [9] have studied MXD-Convection in a pair of L. DRVN enclosure full of with copper-water nano-fluid. From the findings, it was deduced that the consecutive arrangement of the two lids generates an augmented shear force, aligning with the buo yancy force within the cavity, is the best scenario for achieving a high heat transfer rate.

In their numerical study, Wenning Zhouab and Yuying Yan [10] focused on analyzing the MXD-Convection occurring within a double L. DRVN cubic cavity under differential heating conditions. Through their simulations, to investigate the influence of lid directions and heat sources on the heat transmission physical characteristics of the system. The finding of their study revealed that the orientation of the lids and the arrangement of heat sources played a significant role in influencing the heat transmission process. The interaction between the L. DRVN and buoyancy-driven flows within the cubic cavity led to complex flow patterns. It was detected that the heat transmission rate varied depending on the specific configuration of the lid directions and heat sources.

Esfe, et al. [11] developed two-dimensional MXD-convection in an enclosure with two movable lids. Their analysis revealed the presence of two principal vortices within the streamlines when the moving lids exert opposing effects. Furthermore, the results demonstrated that the intensity of these vortices, which align with the buoyancy force, increased with higher Richardson numbers.

Billah, et al. [12] explored mixed-convection within a cavity featuring a centrally positioned, hollow, circular cylinder undergoing heating. Their findings underscored a significant dependence analyzing the flow field and temperature distribution along with variations in both the cylinder diameter and the solid-fluid ratio of thermal conductivity across the three distinct convective states

Islam, et al. [13] Examined MXD-Convection in a square enclosure a block. The block is heated while being exposed to a hot temperature, while the side walls of the hollow area are kept at a cold temperature. The behavior the heat transmission that occurs inside the enclosure as a function of the government parameters, notably the Richardson number, the ratio dimensions of the block, and its eccentricity, were the authors' main concerns. The findings demonstrate that, for a small block size, an increase the Richardson number does not impact on the heat transport.

Aparna Vijayan, et al. [14] recently conducted a study focusing on MXD-Convection in a tall L. DRVN hollow featuring a triangular heat source. The study is conducted to illustrate the behavior of convection in tall cavities with distinct aspect ratios, at various Richardson numbers, power-law indices for non-Newtonian fluids, and Prandtl numbers, for a constant Grash of number of 10^4. They observed that the flow circulation is confined near the region of the moving wall, nevertheless of the Richardson number for low Prandtl numbers.

Regardless of the extensive research on convection [15, 17] within enclosed spaces for different designs and boundaries, there has been little focus on investigating MXD-convection within a lid driven 3D. Enclosed space containing a heated block. This particular setup is extremely useful for simulating practical situations involving heat absorption or generation. What distinguishes this study from previous research efforts is its use of a blend of proactive and passive techniques to effectively manage and control the flow and heat transfer.

2. MATHEMATICAL FORMULATION

As illustrated in Figure1, her issues being looked up one tails a three-dimensional cavity containing Alumina nano-fluid, presumed to possess incompressible and Newtonian properties. Additionally, the movement is characterized as laminar and single-phase, with the neglect of Brownian. The cavity has an isothermal block at the right (Hot temperature) and the left vertical wall is assumed to have a fixed temperature (cold temperature). The remaining walls are assumed to be insulated. The left wall is in motion with a velocity represented by $v = V_0$. The thermophysical properties of the utilized nano-fluid, as detailed by Horasan Izadeh, et al. (2013), are presented in Table 1 presumably all these properties remain constant.

Table 1. Thermophysical characteristics of alumina and water at T=300 K

	k (W/Km)	C_p (J/KgK)	ρ (Kg/m^3)	α (m^2/s)	β (K^{-1})
Water	0.613	4179	997.1	1.47×10^{-7}	21×10^{-5}
Alumina	40	765	3970	-	0.85×10^{-5}

The dimensional continuity, energy and momentum equations can be formulated as follows, considering the aforementioned assumptions (Selimefendigil and Oztop, (2016); Selimefendigil and Chamkha, [18]):

Equation of continuity:

$$\frac{\partial w}{\partial z}+\frac{\partial u}{\partial x}+\frac{\partial v}{\partial y}=0 \tag{1}$$

- Equation of momentum x:

$$\frac{\partial (uu)}{\partial x}+\frac{\partial (vu)}{\partial y}+\frac{\partial (wu)}{\partial z}=-\frac{1}{\rho_{nf}}\frac{\partial p}{\partial x}+v_{nf}\left(\frac{\partial^2 u}{\partial x^2}+\frac{\partial^2 u}{\partial y^2}+\frac{\partial^2 u}{\partial z^2}\right) \tag{2}$$

- Equation of momentum y:

$$\frac{\partial (uv)}{\partial x}+\frac{\partial (vv)}{\partial y}+\frac{\partial (wv)}{\partial z}=-\frac{1}{\rho_{nf}}\frac{\partial p}{\partial y}+ +v_{nf}\left(\frac{\partial^2 v}{\partial x^2}+\frac{\partial^2 v}{\partial y^2}+\frac{\partial^2 v}{\partial z^2}\right)+ +\frac{(\rho\beta)_{nf}}{\rho_{nf}}g(T-T_{ref}) \tag{3}$$

- Equation of momentum z:

$$\frac{\partial (uw)}{\partial x}+\frac{\partial (vw)}{\partial y}+\frac{\partial (ww)}{\partial z}=-\frac{1}{\rho_{nf}}\frac{\partial p}{\partial z}+ +v_{nf}\left(\frac{\partial^2 w}{\partial x^2}+\frac{\partial^2 w}{\partial z^2}+\frac{\partial^2 w}{\partial y^2}\right) \tag{4}$$

- Equation of energy:

$$\frac{\partial (uT)}{\partial x}+\frac{\partial (vT)}{\partial y}+\frac{\partial (wT)}{\partial z}=\alpha_{nf}\left(\frac{\partial^2 T}{\partial x^2}+\frac{\partial^2 T}{\partial y^2}+\frac{\partial^2 T}{\partial z^2}\right) \tag{5}$$

Using after the non-dimensional variables:

$$Z=\frac{z}{L};Y=\frac{y}{L};X=\frac{x}{L};W=\frac{w}{V_0};V=\frac{v}{V_0};U=\frac{u}{V_0};P=\frac{p}{\rho V_0^2}$$
$$\theta=\frac{T-T_c}{T_h-T_c};R_i=\frac{G_r}{R_e^2};G_r=\frac{g\beta L^3\Delta T}{v^2};R_e=\frac{\rho U_p L}{\mu};P_r=\frac{v}{\alpha} \tag{6}$$

We obtain the dimensionless equations:

$$\frac{\partial W}{\partial Z}+\frac{\partial V}{\partial Y}+\frac{\partial U}{\partial X}=0 \tag{7}$$

$$W\frac{\partial U}{\partial Z}+V\frac{\partial U}{\partial Y}+U\frac{\partial U}{\partial X}=-\frac{\partial P}{\partial X}+\frac{v_{nf}}{v_f R_e}\left(\frac{\partial^2 U}{\partial Z^2}+\frac{\partial^2 U}{\partial Y^2}+\frac{\partial^2 U}{\partial X^2}\right) \tag{8}$$

$$V\frac{\partial V}{\partial Y}+U\frac{\partial V}{\partial X}+W\frac{\partial V}{\partial Z}=R_i\frac{\rho\beta_{nf}}{\rho_{nf}\beta_f}\theta+ +\frac{v_{nf}}{v_f R_e}\left(\frac{\partial^2 V}{\partial X^2}+\frac{\partial^2 V}{\partial Y^2}+\frac{\partial^2 V}{\partial Z^2}\right)-\frac{\partial P}{\partial X} \tag{9}$$

$$W\frac{\partial W}{\partial Z}+V\frac{\partial W}{\partial Y}+U\frac{\partial W}{\partial X}=\frac{v_{nf}}{v_f R_e}\left(\frac{\partial^2 W}{\partial X^2}+\frac{\partial^2 W}{\partial Y^2}+\frac{\partial^2 W}{\partial Z^2}\right)-\frac{\partial P}{\partial X} \tag{10}$$

$$W\frac{\partial \theta}{\partial Z}+V\frac{\partial \theta}{\partial Y}+U\frac{\partial \theta}{\partial X}=\frac{\alpha_{nf}}{\alpha_{nf}R_eP_r}+\left(\frac{\partial^2 \theta}{\partial X^2}+\frac{\partial^2 \theta}{\partial Y^2}+\frac{\partial^2 \theta}{\partial Z^2}\right) \tag{11}$$

where, the density ρ_{nf}, specific capacity's heat, thermal expansion coefficient $(\rho\beta)_{nf}$, and thermal diffusivity of the nanofluid α_{nf} are determined by the following expressions:

$$\rho_{nf}=\varphi\rho_s+(1-\varphi)\rho_f \tag{12}$$

$$(C_p\rho)_{nf}=\varphi(\rho C_p)_s+(C_p\rho)_f(1-\varphi) \tag{13}$$

$$(\beta\rho)_{nf}=\varphi(\beta\rho)_s+(\beta\rho)_f(1-\varphi) \tag{14}$$

$$\alpha_{nf}=k_{nf}/(C_p\rho)_{nf} \tag{15}$$

The thermal conductivity and the dynamic viscosity are provided by Maxwell (1891) and Brinkman (1952) respectively:

$$\frac{k_{nf}}{k_f}=\frac{2k_f+k_s-2\varphi(k_f-k_s)}{2k_f+k_s+2\varphi(k_f-k_s)} \tag{16}$$

$$\mu_{nf}=\frac{\mu_f}{(1-\varphi)^{2.5}} \tag{17}$$

The "Nusselt number" is determined by, based on the situation under consideration: The local Nusselt number is calculated for sections (Si) with (i: varies from 1 to 3) as follows:

$$NU_{Si}=\frac{\partial \theta}{\partial k} \tag{18}$$

where, k is perpendicular to the heated plan. A description of the global Nusselt number is as follows:

$$NU_G=NU_{SG1}+NU_{SG2}+NU_{SG3} \tag{19}$$

The average Nusselt numbers on every section, denoted by NU_{SGi}, are as follows:

$$NU_{SG1}=\frac{1}{H\times B}\int_{H-B}^{H}\int_{0}^{H}NU_{S1}dXdZ \tag{20}$$

$$NU_{SG2}=\frac{1}{H\times B}\int_{H-B}^{H}\int_{0}^{H}NU_{S2}dXdZ \tag{21}$$

$$NU_{SG3}=\frac{1}{B\times H}\int_{A}^{H-A}\int_{0}^{H}NU_{S3}dYdZ \tag{22}$$

The dimension less boundary conditions associated to the configuration under study:

- Front and rear sides:

$$U=V=W=0\ ,\ \frac{\partial \theta}{\partial Z}=0 \tag{23}$$

- Top and Bottom sides:

$$U=V=W=0\ ,\ \frac{\partial \theta}{\partial Y}=0 \tag{24}$$

- Left side:

$$U=W=0\,,V=V_0,\ \theta=0 \tag{25}$$

- Right side:

$$0<Y<A;(H-A)<Y<H:\ W=V=U=0,\ \frac{\partial \theta}{\partial X}=0 \tag{26}$$

- At the block:

$$\text{For}:(H-B)\le X\le H;\ A\le Y\le(H-A)$$
$$0\le Z\le H:U=W=0,\ V=V_0\ ,\ \theta=1 \tag{27}$$

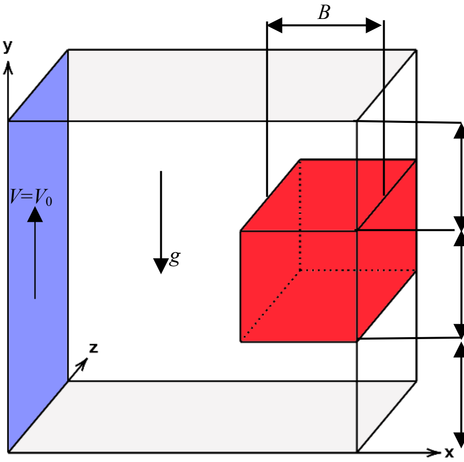

Figure 1. Studied configuration

3. NUMERICAL METHOD AND VALIDATION

The finite volume method was employed to numerically solve the system of partial differential Equations (7)-(11) along with their respective boundary conditions with the power-law technique as described by Patankar [16] in a Fortran programming environment. To couple the pressure and velocity fields, the Van Doormaal and Raithby's SIMPLEC algorithm was employed. The system of algebraic equations obtained was solved iteratively and line-by-line using Thomas's approach, also known as the tri-diagonal matrix algorithm. The convergence of the numerical code was determined by monitoring the residuals of the stream function, and convergence was achieved when these residuals dropped below the specified convergence requirement of 10^{-5}.

In order to obtain reliable and cost-effective results, it is important to select an appropriate grid size that ensures repeatability and accuracy. To determine the temporal global Nusselt number, a series of numerical tests were conducted using different mesh sizes, ranging from (61×61×61) to (101×101×101), as presented in Table 2. This range of mesh sizes was chosen to assess the influence of grid resolution on results and to find optimal balance between accuracy and computational costs.

To ensure a balance between computational cost and research accuracy, a grid size of (81×81×81) was selected for the current study. This particular grid size was deemed appropriate to achieve reliable results without imposing excessive computational demands. The values of (R_e=100, R_i=1, and ε=40%) were specifically chosen, providing a well-defined set of conditions for the investigation, after conducting a series of tests for various combinations of R_e, R_i and block dimensions ε values for the parameter (Φ=0).

Table 2. Effect of the grid size on the global number's Nusselt for the block (case R_e=100, R_i=1, Φ=0% and ε=40%)

Grid size	61×61×61	71×71×71	81×81×81	91×91×91	101×101×101
Nu_{globl}	13.5602	12.6731	12.4889	12.4259	12.90834

In the context of validating our code. we conducted several comparisons with various results from well-known researchers, including:

Table 3 Presents the validation results of the average Nusselt number for pure water. and aluminum oxide-water. These results were compared with those obtained by Ravnik, et al. [18] for different Rayleigh numbers. confirming the accuracy and reliability of the numerical code used in this study.

Furthermore, the code's performance in simulating mixed-convection was verified through comparisons with the findings of the velocity $V(X)$ and $U(Y)$ between our results and those of Ravnik, et al. [18]. Additionally, Table 4 confirms a good agreement of the results with those of Iwatsu, et al., Ravnik, et al. and ours.

Table 3. Rayleigh numbers are compared to the average number's Nusselt

	Water pure (Φ=0%)			Al_2O_3-water (Φ= 0.01)		
	Present work	Ref. [18]	Discrepancy ratio (%)	Present work	Ref. [18]	Discrepancy ratio (%)
$R_a=1\times10^3$	1.079	1.071	0.74	1.358	1.345	0.96
$R_a=10\times10^3$	2.104	2.078	1.23	2.181	2.168	0.60
$R_a=100\times10^3$	4.601	4.510	1.98	4.894	4.806	1.80
$R_a=1000\times10^3$	9.285	9.032	2.72	10.027	9.817	2.09

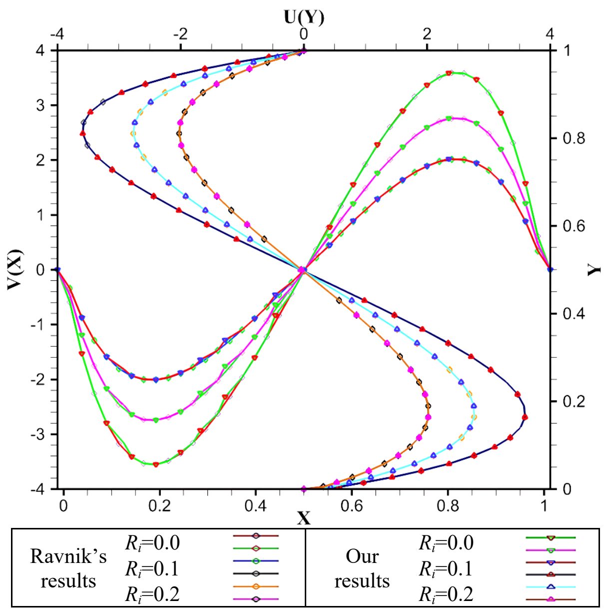

Figure 2. Comparison of the velocity $U(x)$ and $V(x)$ between our results and those of Ravnik, et al. [19]

Table 4. Comparison of the current solution's average Nusselt number at thee top surface with Iwatsu and al.'s for a vertical cavity at Gr=100 Chamkha and associates

	Iwatsu, et al. [20]	Chamkha, et al. [21]	Current data
$R_e=1\times10^2$	1.94	2.01	1.98
$R_e=4\times10^2$	3.84	3.91	3.88
$R_e=10\times10^2$	6.33	6.33	6.30

4. RESULTS AND DISCUSSIONS

The impact of thermal and geometrical parameters on fluid flow and heat transfer in a three-dimensional cavity are investigated numerically. Through streamlines temperature dispersion and the overall Nusselt number resulting thermal and flow patterns are analyzed over a wide range of Reynolds numbers ($10\leq R_e\leq200$). Richardson numbers ($0\leq R_i\leq10$). heating surface dimensions ($0.2\leq\varepsilon\leq0.7$). and nanoparticle solid volume fractions ($0\%\leq\Phi\leq4\%$). The temperature distribution inside a three-dimensional cavity at different Reynolds numbers R_e. for (ε=40%, R_i=0.1, Φ=0%) is shown in Figure 3. The representation demonstrates the way fluids move from the heated block to the chilly wall. Maintaining the cavity's rate of heat transfer. The high thermal gradients in the active wall at the given ε value cause this convective phenomenon. The energy emitted by the heat transfer fluid rises in proportion to the Reynolds number.

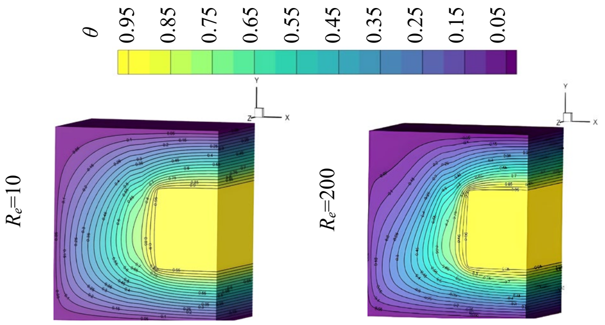

Figure 3. 3D temperature distribution for R_e=10 and R_e=200

Several planes were considered in order to improve our understanding of the three-dimensional temperature profile inside the cavity. The plane (Z=0.5) illustrates as the most accurate plane within the cavity. Figures 4 to 6 depict the results obtained for different parameter settings except for the heating block dimension (ε), which was kept constant at a value of 40% throughout the analyses. In Figure 4, the variations in temperature distribution and flow patterns are displayed for different Reynolds numbers, ranging from (10 to 200), for different volume fraction of nanoparticles (Φ=0%, Φ=2% and Φ=4%), and for a constant value of Richardson number (R_i=0.1). The results demonstrate an interesting behavior when considering a low Reynolds number (R_e=10). At this condition, the fluid flow within the cavity is primarily driven by the movement of the lid from the left side. The observed flow pattern resembles a clockwise rotation occurring at the middle of the left side of the cavity. This phenomenon is attributed to natural convection, where temperature difference induces fluid movement, thus creating characteristic vortices and flow patterns. The clockwise rotation from the correlation between the position of the lid and the geometry of the cavity, thereby inducing a circular motion of the fluid at the specific location.

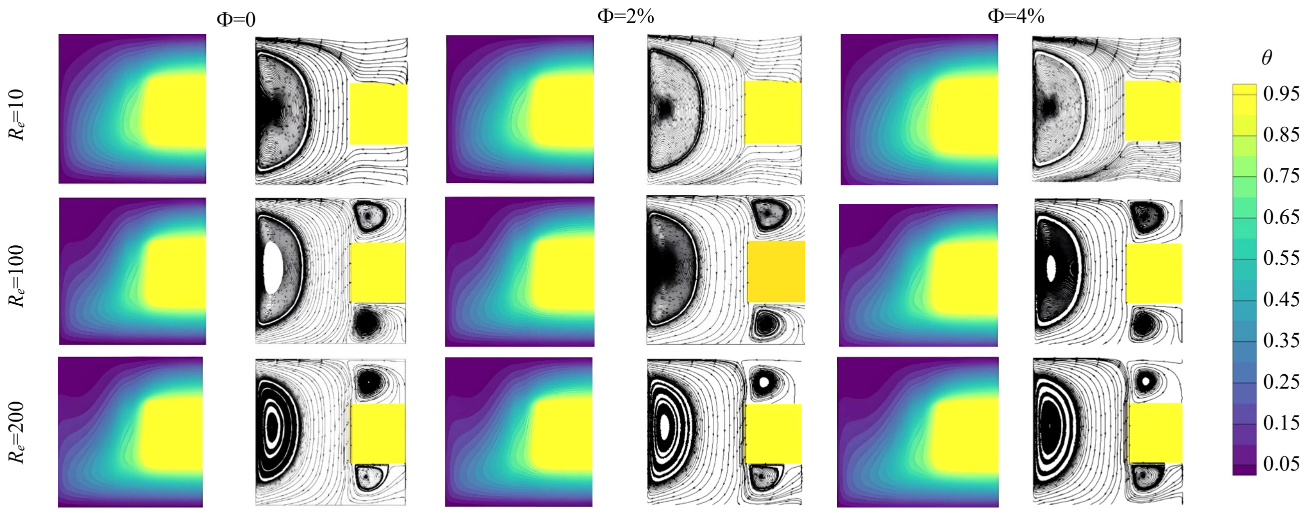

Figure 4. Isotherms and isolines in the plan Z=0.5, for pure water and water +Al_2O_3 for R_i=0.1 and different value (R_e=10, R_e=100 and R_e=200), ε=40% and (with Φ=0, Φ=2% and Φ=4%)

Additionally, the fluid flow is characterized by its slow velocity, which result in laminar flow patterns and minimal disturbance to the flow lines. The preservation of line shapes indicates a stable flow regime, where the inertial forces are negligible compared to viscous forces. The slow velocity causes the open lines to maintain the same shape throughout the rest of the cavity, where the inertial forces are negligible compared to viscous forces. Therefore, despite the movement induced by the lid, the overall flow remains relatively uniform and predictable within the cavity.

Analyzing the isotherms within the cavity reveals specific temperature distribution patterns. The high-temperature region is predominantly concentrated and stratified near the vicinity of the heating block. This concentration signifies that the heat generated by the block is mostly retained in this region. Furthermore, the isotherm lines corresponding to lower and medium temperatures appear to be parallel to each other in other areas of the cavity. The observed parallel arrangement suggests the occurrence of thermal forced convection heat transfer within these specific regions. Thermal forced convection describes the process by which heat is transferred due to fluid movement induced by a temperature gradient. The presence of parallel flow lines indicates the formation of thermal boundary layers along the surfaces, facilitating heat transfer from the solid boundaries to the fluid through convection.

This phenomenon adheres to Newton's law of cooling, wherein the rate of heat transfer is directly proportional to both the temperature differential between the solid surface and the fluid and the convective heat transfer coefficient. With an increase in the Reynolds number to a moderate value (R_e = 100), the fluid flow undergoes a transition, resulting in the formation of two counter clockwise vortices at the top and bottom of the heated block. This transition is attributed to dynamic's fluid, where variation in the Reynolds number alter the balance between inertial forces and viscous forces in the flow. At moderate Reynolds numbers, the accelerated forced flow induces instability in the fluid motion, leading to the formation of vortices. These vortices serve to redistribute momentum and energy within the flow, influencing heat transfer and mixing processes. With a further increase in Reynolds number to (R_e=200), these vortices become larger and more intense, while the anti-clockwise vortex on the left side expands to occupy the entire cavity.

The temperature distribution demonstrates that lower values are associated with the isotherms directed towards the heated block, but a distortion of the temperature iso-lines in the core of the cavity indicates the influence of inertia forces on flow transport. Regardless of the parameters being considered, one consistent observation is that increasing the volume fraction of nanoparticles has a positive impact on heat transfer within the system. This improvement can be attributed to the enhanced thermal conductivity of the fluid, the changes in fluid flow behavior, and the additional convective flows induced by nanoparticles. Furthermore, Increasing the volume fraction of nanoparticles for all Reynolds numbers leads to an improvement in the heat transfer by altering the fluid's thermal conductivity and convective properties. However, the impact is limited due for low Reynolds number by restricting the fluid motion.

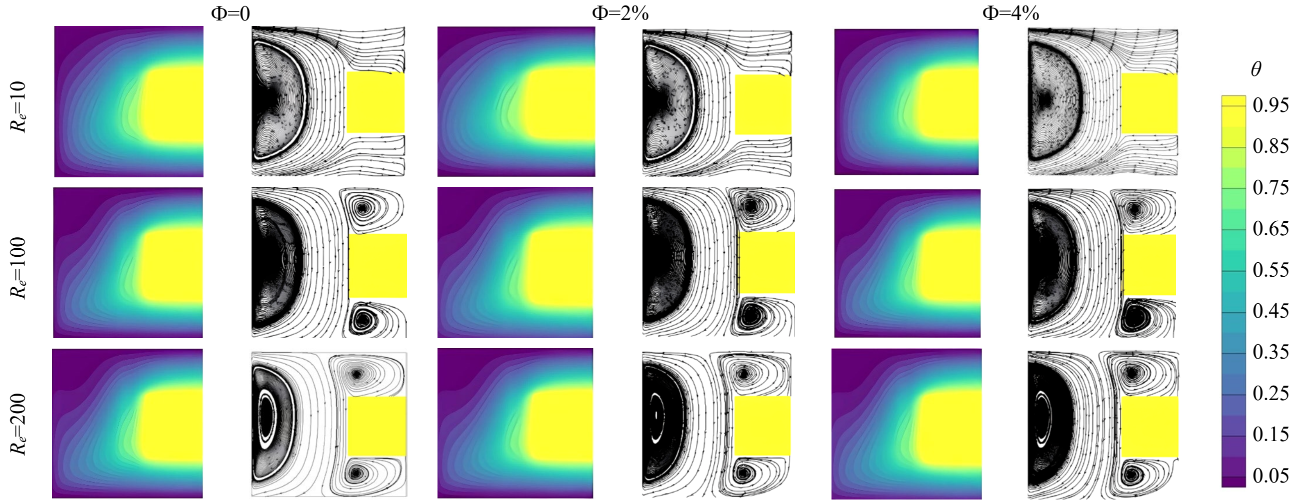

Figure 5. Isotherms and isolines in the plan Z=0.5 for pure water and water+Al2O3 for R_i=1 and different values of (R_e=10, R_e=100 and R_e=200), ε=40% and (Φ=0, Φ=2% and Φ=4%)

When the Richardson number increases to (R_i=1), as shown in Figure5., and for all Reynolds number, the behavior of the streamlines and isotherm lines exhibits similarities to the previous case with a Richardson number (R_i=0.1). However, there are slight differences observed. In this scenario, the interaction between the lid-driven flow and the heated block remains relatively weak, preventing significant variations in fluid density and limited particle movement. Consequently, the effect of nanoparticles on the flow behavior and heat transfer is minimal at this stage.

Examining the isotherm lines, a noticeable change occurs around the heated surface. The isotherms become progressively tightened, indicating a higher temperature gradient near the heated surface. Additionally, these isotherm lines assume a nearly vertical orientation in the remaining areas of the cavity. This behavior can be attributed to the thermal interaction between the buoyancy effect generated by the heated surface and the incoming cold flow. The interplay between these factors allows for the development of mixed convection, where both forced and natural convection contribute to heat transfer.

Moreover, for (R_i=1), increasing the volume fraction of nanoparticles from (Φ=0% to Φ=4%) influence the balance between buoyancy-driven and forced convection by altering fluid properties such as density and viscosity. This led to changes in flow behavior and heat transfer efficiency.

At a higher Richardson number (R_i=10), as depicted in Figure 5, the influence of natural convection within the cavity becomes more pronounced. this phenomenon can be explained as: When the Richardson number increases, buoyancy forces become more dominant compared to externally forced flow. As a result, the temperature gradient created by the heated block induces convective currents within the fluid. These convective currents disrupt the initially established flow patterns, leading to the formation of rotating cells. The clockwise rotation of these cells on the left side of the heated block is a consequence of the interaction between buoyancy-driven flow and the geometry of the cavity. In the case of a small Reynolds number (R_e=10), the temperature lines appear to be uniformly distributed.

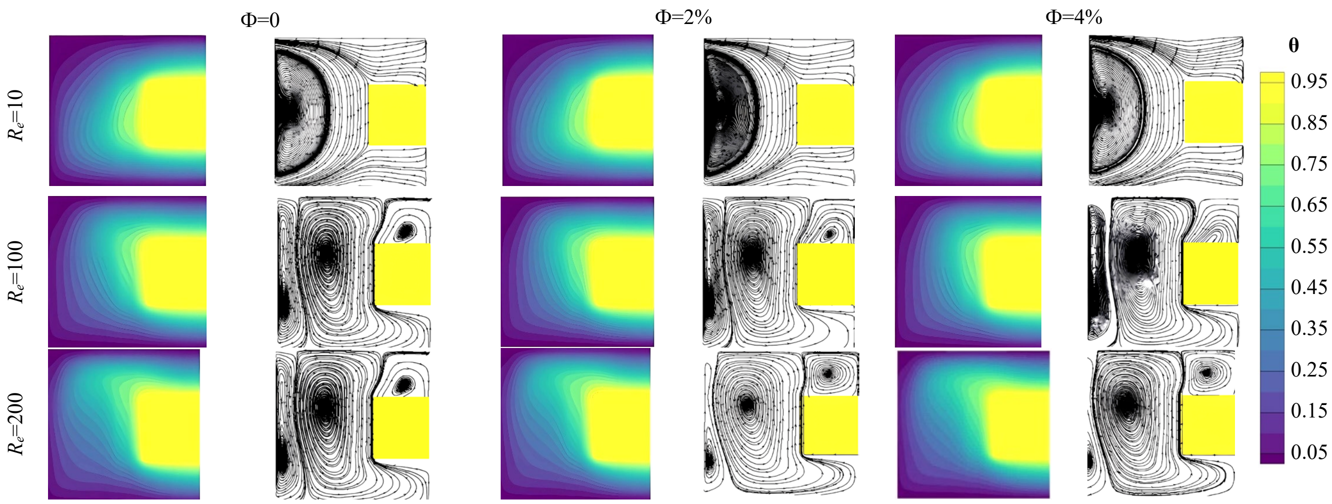

Figure 6. Isotherms and isolines in the plan Z=0.5 for pure water and water+Al_2O_3 for R_i=10 and different value of (R_e=10, R_e=100 and R_e=200), ε=40% and (Φ=0. Φ=2% and Φ=4%)

The isotherms near the heated block become vertically compressed, suggesting a more concentrated heat exchange in that region. Additionally, a slight deviation of the isotherms can be observed on the upper part of the cavity, indicating enhanced convective heat exchange. In contrast, the lower part of the cavity remains at a uniform cold temperature, creating a thermally inactive zone. This zone expands as the flow motions intensify.

As the Reynolds number increases to a moderate value of (R_e=100), a remarkable phenomenon occurs. A distinct vortex manifests within the cavity, occupying the central region of the hallway and extending to the bottom of the block. The formation and positioning of this vortex are directly influenced by the interplay between buoyancy and shear forces. As the Reynolds number further increases to (R_e = 200), the central anti-clockwise vortex grows in size and intensity, while the cell on the left side begins to disappear. Furthermore, the boundary layers near the heated block become thinner, allowing a portion of the internally heated fluid to interact favorably with the driven cold flow and the cold wall. This interaction is facilitated by the dominant buoyancy effects, which become the primary mode of mixed convection transport.

Physically, the increase in Reynolds number, involves the dominance of inertial forces over viscous forces which amplifies fluid motion, leading to the formation of vortices. The interplay between buoyancy and shear forces determines the positioning and intensity of these vortices. As Reynolds number rises, the enhanced fluid motion disrupts the existing flow patterns, influencing the distribution of temperature gradients and the development of vortices. The thinning of boundary layers near the heated block facilitates enhanced mixing between the heated and cold fluids, driven primarily by buoyancy effects.

5. HEAT TRANSFER

To assess the heat transfer performance in the examined configuration, we investigate the changes in the global average Nusselt numbers across the three sections of the heated block as a function of Richardson (R_i), volume fraction of the nanoparticle and dimension of the block ε values, considering different Reynolds numbers. The results are presented in Figures 7-9.

Clearly as the volume fraction of nano-fluid particles and Reynolds numbers increase. the Nusselt number also increases for all considered dimensions of the heating block. denoted as ε. However. when the Reynolds number exceeds (R_e>40). there is a slightly noticeable difference in the Nusselt number for all volume fractions of nanoparticles. Additionally. for all Reynolds numbers. an increase in the dimensions of the heated block leads to a higher global Nusselt number.

When the Richardson number is increased for a fixed dimension of the heated block. there is a minor variation in the global Nusselt number. This can be attributed to the weak interaction between inertia and buoyancy effects. leading to a gradual progression of MXD-Convection. Consequently, heat transfer near the heating sections of the block is primarily governed by conduction rather than convection. exists between the proportion (ε%) of the source of heat and the average Nusselt number.

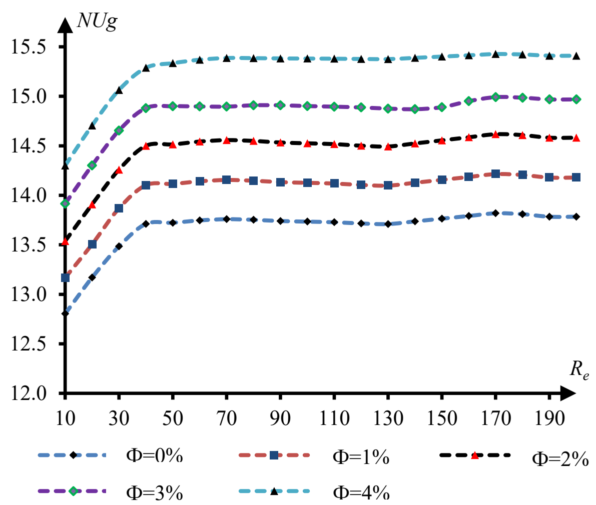

Figure 7. The impact of the volume fraction of nanoparticle Φ and Reynolds numbers on the overall Nusselt number when R_i=0.1 and ε=40%

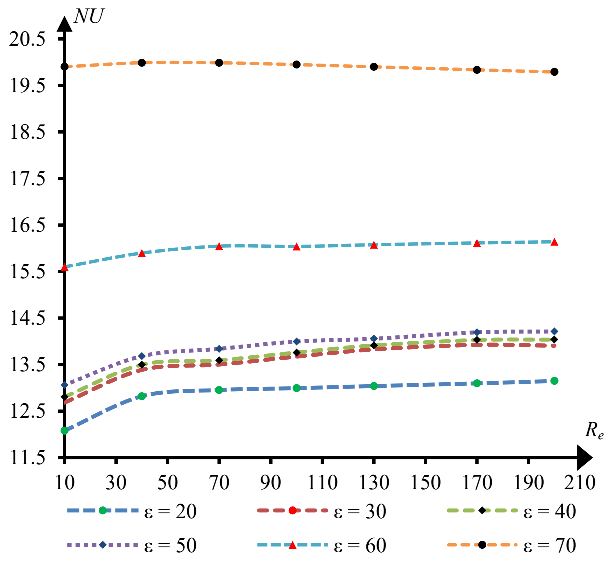

Figure 8. The impact of the block dimension section ε and Reynolds numbers on the overall Nusselt number when R_i=1 and Φ=1%

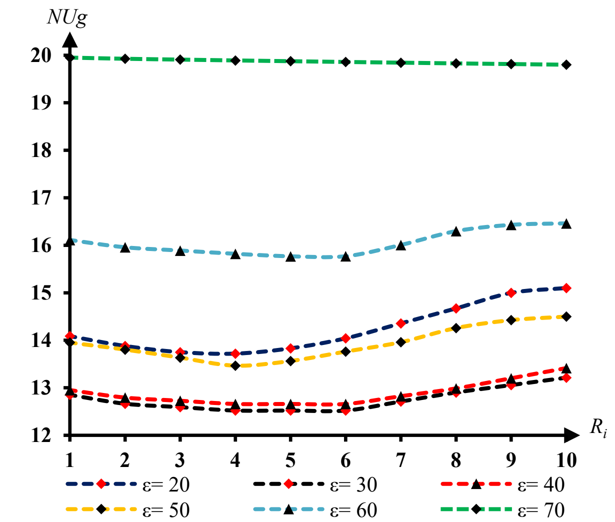

Figure 9. The impact of the block dimension section ε and number's Richardson on the overall number's Nusselt when R_e=100, and Φ=1%

6. CONCLUSION

The focus of the current research is to investigate the numerical simulation of mixed convection phenomena in a lid-driven cavity filled with nanofluid. The present study methodically examines the mixed convection caused by the left cavity wall's movement while taking into account the impact of the nanofluid on the heated block's cooling process. In this study we explore how important variables, such as the dimension of the heat source, Reynolds number, and volume fraction of nanofluid, affect the heat transfer inside the cavity.

In summary, the principal findings of this study are as follows:

- A higher volume fraction results in increased heat exchange and flow intensity.
- The fluid flow appears as a large cell occupying almost the whole middle of the cavity when $R_i \geq 1$, indicating the importance of free convection inside the cavity.
- Optimizing heat transfer can be achieved by utilizing geometry parameters, such as the dimensionless height and width of the heat source. Interestingly, there is a positive correlation between the average Nusselt number and the portion (ε%) of the heat source.
- The inertia force becomes more significant as the Reynolds number rises. which raises the maximum flow function of both the pure fluid and the nano-fluid. For $R_e \geq 50$. the flow is stronger when nano-fluid is present than when the fluid is pure.
- According to all of the earlier research. the scenario where the portion of the block is set at ε=40% is the one that enhances thermal and dynamic transfers. It can be asserted that this represents the most favorable portion.

NOMENCLATURE

1. Acronyms

MXD-Convection	Mixed Convection
L.DRVN	Lid Driven

2. Symbols and Parameters

Cp: Specific heat capacity, [J×Kg^{-1}×K^{-1}]
g: Gravitational acceleration, [ms^{-2}]
G_r: Grashof number
k: Thermal conductivity, [W/m×K]
L: Characteristic length, [m]
Nu: Nusselt number
P_r: Prandtl number
R_a: Rayleigh number
R_e: Reynold number
R_i: Richardson number
P: Dimensionless pressure
T: Temperature, [K]
V_0: Lids velocity, [m/s]
u, v, w: Velocity components, [m/s]
U, V, W: Dimensionless velocity, $(u, v, w)/V_0$
x, y, z: Space coordinates, [m]
X, Y, Z: Dimensionless space coordinates $(x, y, z)/L$
α: Thermal diffusivity, [m^2×s^1]
β: Coefficient of thermal expansion, [K^1]
μ: Dynamic viscosity, [kg×m×s]
Φ: Volume fraction of nanoparticles
ε: Heating block dimension
u: Dimension less temperature
v: Kinematic viscosity, [m^2 s^1]
ρ: Density, [kg m^3]
θ: Temperature thermal expansion coefficient
c: Cold
f: Fluid
h: Hot
nf: Nanofluid
s: Solid

REFERENCES

[1] N. Ben Cheikh, A.J. Chamkha, B. Ben Beya, T. Lili, "Natural Convection of Water-Based Nano-Fluids in a Square Enclosure with Non-Uniform Heating of the Bottom Wall", J. Modern Phys., Vol. 4, No. 2, pp. 147-159, 2013.

[2] F.I. Doshmanziari, A.E. Zohir, H.R. Kharvani, D. Jalali Vahid, M.R. Kadivar, "Characteristics of Heat Transfer and Flow of Al_2O_3/Water Nano-Fluid in a Spiral-Coil Tube for Turbulent Pulsating Flow", Heat Mass Transf., Vol. 52, No. 7, pp. 1305-1320, 2016.
[3] H. Messaoud, B. Meziani, D. Sadaoui, "Numerical Study of Mixed Convection and Flow Pattern in Various Across Shape Concave Enclosure", International Journal of Heat and Technology, Vol. 35, No. 3, pp. 567-575, 2017.
[4] E. Fontana, C.A. Capeletto, A. Da Silva, V.C. Mariani, "Numerical Analysis of Mixed Convection in Partially Open Cavities Heated from Below", International Journal of Heat and Mass Transfer, Vol. 81, pp. 829-845, 2015.
[5] R. Iwatsu, J.M. Hyun, K. Kuwahara, "Mixed Convection in a Driven Cavity with a Stable Vertical Temperature Gradient", Int. J. Heat Mass Transfer, Vol. 36, pp. 1601-1608, 1993.
[6] H. Doghmi, B. Abourida, H. Belarche, M. Sannad, M. Ouzaouit, "Effect of the Inlet Opening on Mixed Convection Inside a Three-Dimensional Ventilated Cavity", Thermal Science International Scientific Journal, 2017.
[7] E. Abu Nada, A.J. Camkha, "Mixed Convection Flow in a Lid-Driven Inclined Square Enclosure Filled with a Nano-Fluid", European Journal of Mechanics, B/Fluids, Vol. 29, Issue 6, pp. 472-482, 2010.
[8] M.A. Sheremet, I. Pop, "Mixed Convection in a Lid-Driven Square Cavity Filled by a Nano-Fluid", Buongiorno's Mathematical Model, Applied Mathematics and Computation, Vol. 26, No. 6, pp. 792-808, 2015.
[9] S. Nouari, S. Eihamdani, A. Bendou, E. Bara, "Three-Dimensional Numerical Simulation of Mixed Convection of Nano-Fluid Inside a Double Lid Driven Differentially Heated Cavity", AIP Conference Proceedings, Vol. 23, p. 45, 2021.
[10] B.Z. Wenning, Y. Yuying, L. Boltzmann, "Simulation of Mixed Convection of Nano-Fluid with Different Heat Sources in a Double Lid Driven Cavity", International Communication in Heat and Mass Transfer, Vol. 97, pp. 39-46, October 2018.
[11] M.H. Esfe, A.Z. Ghadi, M.N. Javad, "Numerical Simulation of Mixed Convection Within Nano-fluid-Filled Cavities with Two Adjacent Moving Walls", Transactions of the Canadian Society for Mechanical Engineering, Vol. 37, No. 4, 2013.
[12] M.M. Billah, M.M. Rahman, U.M. Sharif, N.A. Rahim, R. Saidur, M. Hasanuzzaman, "Numerical Analysis of Fluid Flow Due to Mixed Convection in a Lid-Driven Cavity Having a Heated Circular Hollow Cylinder", Int. Commun. Heat Mass Transfer, Vol. 38, pp. 1093-1103, 2011.
[13] A.W. Islam, M.A.R. Sharif, E.S. Carlson, "Mixed Convection in a Lid Driven Square Cavity with an Isothermally Heated Square Blockage Inside", International Journal of Heat and Mass Transfer, Vol. 55, No. 19-20, pp. 5244-5255, 2012.
[14] V. Aparna, M. Krunal Gangawane, "Mixed Convection in a Tall Lid-Driven Cavity with a Triangular Heat Source for Non-Newtonian Power-Law Fluids", Journal Therm. Anal. Calorim., 2020.
[15] A. Maanser, A. Benouis, M. Gherdoui, R. Boudjadja, "Effect of Temperature on Mechanical Properties of Mortars with Incorporation of Different Chemical Admixtures", International Journal on Technical and Physical Problems of Engineering (IJTPE), Issue 51, Vol. 14, No. 2, pp. 330-338, June 2022.
[16] H. Chekenbah, A. El Abderrahmani, A. Aghanim, Y. Maataoui, R. Lasri, "Solving Problem of Partial Shading Condition in a Photovoltaic System Through a Self-Adaptive Fuzzy Logic Controller", International Journal on Technical and Physical Problems of Engineering (IJTPE), Issue 47, Vol. 13, No. 2, pp. 130-137, June 2021.
[17] K. Bouzid, L. Belarche, B. Abourida, A. Siadi, "Numerical Investigation of Hybrid Nanofluid MHD Mixed Convection Inside a Three-Dimensional L-Shaped Cavity", International Journal on Technical and Physical Problems of Engineering (IJTPE), Issue 60, Vol. 16, No. 3, September 2024.
[18] J. Ravnik, L. Skerget, M. Hribersek, "Analysis of Three-Dimensional Natural Convection of Nano-Fluids", BEM. Engineering Analysis with Boundary Elements, Vol. 34, No. 12, pp. 1018-1030, 2010.
[19] S.V. Patankar, "Numerical Heat Transfer and Fluid Flow", McGraw Hill, New York, USA, 1980.
[20] R. Iwatsu, J.M. Hyun, K. Kuwahara, "Mixed Convection in a Driven Cavity with a Stable Vertical Temperature Gradient", Int. Heat Mass Transfer, Vol. 25, No. 0882#0590Ð0597, 2010.
[21] A.J. Chamkha, K.M. Khanafer, "Int. Heat Mass Transfer", Vol. 31, No. 0888#1354D1370, 2003.

BIOGRAPHIES

<u>Name</u>: **Ali**
<u>Surname</u>: **Siadi**
<u>Birthday</u>: 15.12.1970
<u>Birthplace</u>: Errachidia, Morocco
<u>Bachelor</u>: Physics and Electronics, Mohamed V University, Rabat, Morocco, 1994
<u>Master</u>: Energy, Process and Energy Engineering, National School of Applied Science (ENSA), Ibn Zohr University, Agadir, Morocco, 2011
<u>Doctorate</u>: Student, Energy, Fluid Mechanics, Energetics, and Thermo-dynamics, National School of Applied Science (ENSA), Ibn Zohr University, Agadir, Morocco, Since 2019
<u>The Last Scientific Position</u>: Chief Engineer CRMEF, Taroudant, Morocco, Since 1995
<u>Research Interests</u>: Computational Study and Investigation of Diverse 3D Flow Patterns: Laminar and Turbulent Flow Behaviors with Nanofluids in Ventilated Enclosures
<u>Scientific Publications</u>: 5 Papers, 2 Books, 1 Project

Name: **Lahoucine**
Surname: **Belarche**
Birthday: 27.03.1968
Birthplace: Tiznit, Morocco
Bachelor: Mechanical Engineering, ENSET, University Mohamed V, Rabat, Morocco, 2008
Master: Energy, Process and Energy Engineering, National School of Applied Science (ENSA), Ibn Zohr University, Agadir, Morocco, 2010
Doctorate: Energy, Fluid Mechanics, Energetics, and Thermo-Dynamics, National School of Applied Science (ENSA), Ibn Zohr University, Agadir, Morocco, 2015
The Last Scientific Position: Prof., Mechanical Engineering, Department of Mecanics, Processes, Energy and Environement, National School of Applied Science (ENSA), Ibn Zohr University, Agadir, Morocco, Since 2017
Research Interests: Heat and Mass Transfer and its Application in Mechanical and Industrial Engineering, Cooling of Electronics and Mechanical Components, Drying Technologies, Solar Collectors
Scientific Publications: 22 Papers, 2 Books, 5 Projects, 1 Thesis

Name: **Btissam**
Surname: **Abourida**
Birthday: 05.12.1974
Birthplace: Marrakesh, Morocco
Bachelor: Physics, Energy and Fluid Mechanics, Faculty of Sciences, Cadi Ayyad University, Marrakech, Morocco, 1993
Master: Physics, Energy and Fluid mechanics, Faculty of Sciences, Cadi Ayyad University, Marrakech, Morocco, 1995
Doctorate: Physics, Energy and Fluid Mechanics, Faculty of Sciences, Cadi Ayyad University, Marrakech, Morocco, 1999
The Last Scientific Position: Prof., Mechanics and Energy, Faculty of Sciences, Cadi Ayyad University, Marrakech, Morocco, Since 2020
Research Interests: Heat and Mass Transfer, and Energy
Scientific Publications: 24 Papers, 10 Books, 5 Projects, 1 Thesis

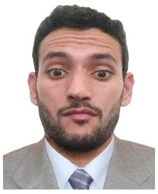

Name: **Kamal**
Surname: **Bouzid**
Birthday: 25.12.1992
Birthplace: Ouarzazate, Morocco
Bachelor: Mechanical Engineering, Industrial Product Design, ENSET, Mohamed V University, Rabat, Morocco, 2014
Master: Mechanics, Mechanical Engineering, ENSET, Mohamed V University, Rabat, Morocco, 2016
Doctorate: Student, Mechanics, Processes, Energy and Environement, Natural and Mixed Convection within Basic and Elaborate Enclosures, LMPEE, Faculty of UIZ, National School of Applied Science (ENSA), Agadir, Morocco, Since 2019
The Last Scientific Position: Lecturer, Industrial and Mechanical Engineering, Ministry of Education and Sport, Agadir, Morocco, Since 2018
Research Interests: Mechanical Engineering, Heat and Mass Transfer, Production Process Optimization
Scientific Publications: 2 Papers, 1 Book, 1 Project